SCIENTIFIC REPORTS

OPEN

SUBJECT AREAS:
BIOTECHNOLOGY
MATERIALS
CELL BIOLOGY
STEM CELLS

Received
23 August 2011

Accepted
31 January 2012

Published
17 February 2012

Correspondence and requests for materials should be addressed to S.S. (silvia.scaglione@cnr.it)

Order versus Disorder: in vivo bone formation within osteoconductive scaffolds

Silvia Scaglione[1,2], Paolo Giannoni[1], Paolo Bianchini[3], Monica Sandri[4], Roberto Marotta[3], Giuseppe Firpo[5], Ugo Valbusa[5], Anna Tampieri[4], Alberto Diaspro[3], Paolo Bianco[6] & Rodolfo Quarto[1,7]

[1]Advanced Biotechnology Center (CBA), Largo R. Benzi 10, 16145 Genoa, Italy, [2]IEIIT – Research National Council (CNR), Via De Marini 6, 16149 Genoa, Italy, [3]Italian Institute of Technology, Via Morego 30, 16100 Genoa, Italy, [4]ISTEC-CNR, Institute of Science and Technology for Ceramic Materials, National Research Institute, via Granarolo 64, 48018 Faenza, Italy, [5]Nanomed lab, Physics Department (DIFI), Via Dodecaneso, 33 16146 Genova and S.C. Nanobiotecnologie IST, Largo R. Benzi 10, 16132 Genoa, Italy, [6]Department of Molecular Medicine, Sapienza University of Rome, Viale regina Elena 324, 00161 Rome, Italy, [7]Department of Experimental Medicine (DIMES), University of Genoa, Largo R. Benzi 10, 16145 Genoa, Italy.

In modern biomaterial design the generation of an environment mimicking some of the extracellular matrix features is envisaged to support molecular cross-talk between cells and scaffolds during tissue formation/remodeling. In bone substitutes chemical biomimesis has been particularly exploited; conversely, the relevance of pre-determined scaffold architecture for regenerated bone outputs is still unclear. Thus we aimed to demonstrate that a different organization of collagen fibers within newly formed bone under unloading conditions can be generated by differently architectured scaffolds. An ordered and confined geometry of hydroxyapatite foams concentrated collagen fibers within the pores, and triggered their self-assembly in a cholesteric-banded pattern, resulting in compact lamellar bone. Conversely, when progenitor cells were loaded onto nanofibrous collagen-based sponges, new collagen fibers were distributed in a nematic phase, resulting mostly in woven isotropic bone. Thus specific biomaterial design relevantly contributes to properly drive collagen fibers assembly to target bone regeneration.

Several approaches of regenerative medicine involve loading of stem cells onto properly designed biomaterials, with the aim to induce cell differentiation along a pre-defined pathway and to regenerate the target tissue according to physiological cues[1–6]. In bone tissue engineering, stem cells are a key element to achieve tissue regeneration, since few biomaterials are considered osteoinductive[7–11]. Therefore, one of the most intriguing tasks is to obtain materials able to mimic a specific microenvironment, possibly priming the natural process of cell-driven bone regeneration. Chemical composition of the scaffold is crucial: materials that most closely mimic bone chemistry (i.e. hydroxyapatite, tricalcium phosphate) optimally prompt the cellular osteogenic differentiation[4,7,10–13]. Other parameters of scaffold design also influence cell fate, in vitro and in vivo[12,14–20]: to improve the efficiency of biomaterials for bone regeneration, the overall structure and architecture of the scaffold should be appropriate. Indeed, the introduction of porous scaffolds has represented a key achievement in this field[12–16,18–22]. Macroporosity and pathways of pore interconnection have a strong impact on osteogenic outcomes, since high porosity levels are necessary for in vivo bone tissue in-growth, allowing blood vessels invasion and bone matrix deposition in the empty spaces. Although highly porous bioceramics still represent a standard for generating osteoconductive grafts[12,14,15,18], their internal architecture presents some physical constraints (i.e. small pore interconnection size, pore shape). As previously reported[21], these features may limit the physiological blood vessel supply and consequently reduce bone in-growth. In this regard, the use of synthetic/natural polymers as bone substitutes allow scaffolds to be designed and produced without the typical restrictions of mineralized materials. Highly resorbable bone substitutes (i.e. collagen based composites), in fact, represent possible alternative materials, allowing in principle an extended in vivo bone remodeling/deposition over time.

However, it is still unclear whether the pattern and the molecular structure of the newly forming bone might be generated in different ways, based on the structural cues provided by the scaffold design. In the present work, then, we have compared the in vivo cellular response to two osteoconductive materials that maximize differences in internal structure while displaying similar chemical compositions: a highly porous interconnected hydroxyapatite foam (HA)[21] and a hydroxyapatite-collagen composite sponge (HA-Col)[23]. We assessed the pattern of new

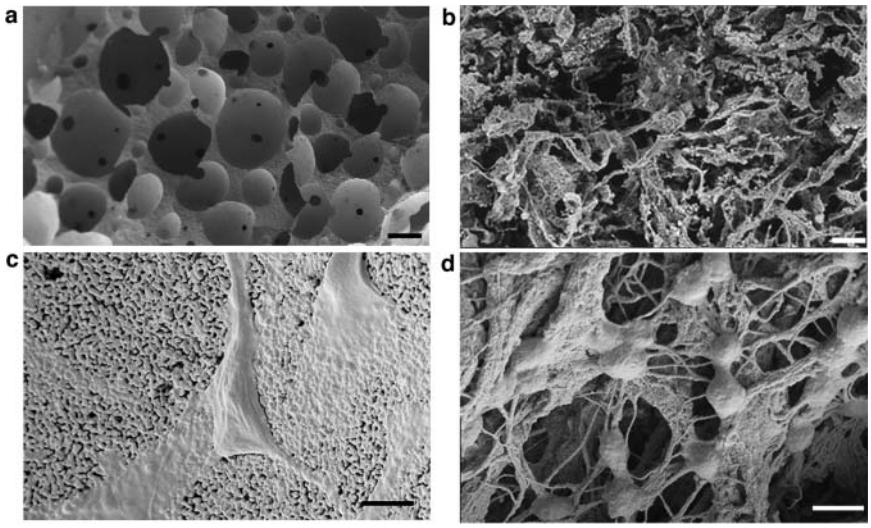

Figure 1 | **Electron microscopic analysis.** Significant differences in terms of micro-nano structure were observed between HA and HA-Col scaffolds (a–c and b–d respectively). At low magnification, HA foams show round-shaped interconnected pores, with black spots representing interconnections between neighbor pores (a). Ha-Col sponge, on the other side, shows a heterogeneous fibrous structure (b). At higher magnification, HA grains clearly form a substrate for cell adhesion, with black spots representing microporosity (c). Ha-Col scaffold highlights cells grasped to the collagen nanofibers (d). Bars: 200 μm, 500 nm respectively.

bone tissue deposited by bone marrow derived cells loaded onto the two scaffolds, ectopically implanted in a murine model, through a combined multimodal 3D optical microscopic analysis.

Results

The micro-nano-structures of the two scaffolds are shown in Fig. 1. At low magnification (Fig. 1a–b), the differences in microarchitecture, pore size and shape between the two scaffolds were evident. In the HA scaffolds, the porosity distribution was bi-modal, being formed by interconnected micro and macropores; the former ones representing the empty inter-grain space, while the latter the macrocavities obtained during the production process. The final porosity of the HA-Col spongy mineralized composites displayed large anisotropic pores, with the largest dimension in the range of 250–450 μm. Both scaffolds had a mean overall porosity close to 80%[21,23]. The interaction of cells and scaffolds is displayed in panels c and d; in HA ceramics the adhesion and spreading of cells onto the material was revealed by morphologically "polarized" cells facing the ceramic surface. Cell interaction with HA-Col evidenced a more complex pattern, characterized by rounded cell bodies in touch with several collagen fibers.

The in vivo bone forming efficiency of the scaffolds was evaluated up to six months after implantation in the ectopic model used (Fig. 2). In agreement with the afore-mentioned cell-biomaterial interactions, bone, in HA, was deposited layer after layer in a polarized fashion, whereas in HA-Col constructs its formation proceeded randomly, without evidences of polarized matrix deposition. In HA scaffolds bone formation started early, with a consistent bone matrix deposition well detectable as early as 1 month after in vivo implantation; almost all pores of the scaffolds were colonized by osteoprogenitor cells which had layered new tissue over the pores surface (data not shown). Mature osteoblasts responsible for bone matrix deposition were lining the newly formed bone surface within the pores. Similarly, 1 month after in vivo implantation, cells loaded onto HA-Col scaffold deposited bone matrix, although with a pattern resembling woven bone, completely embedded within the collagenic matrix of the scaffold (Fig. 2).

Two months after implantation, the amount and pattern of bone tissue within pores were significantly improved in HA scaffolds: bone

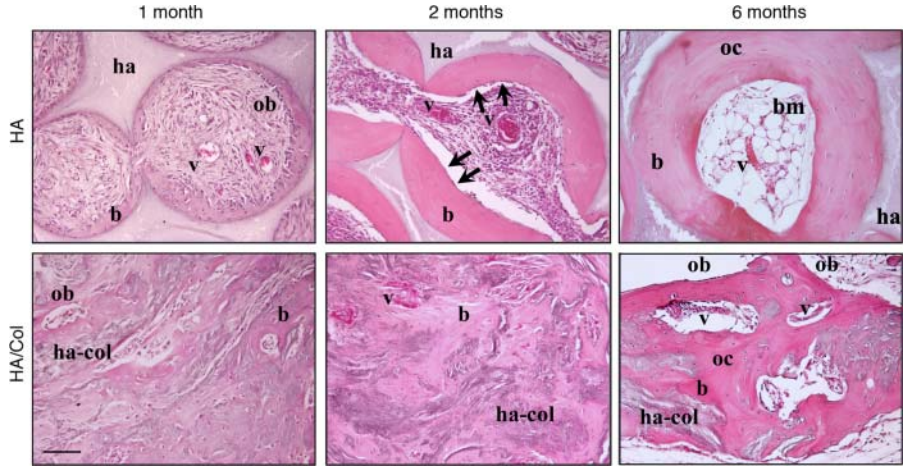

Figure 2 | **Histology of bone tissue.** Pattern of bone tissue deposited by stromal cells within HA and HA-Col grafts. The histological analysis was performed 1–2–6 months after implantation. b: bone; bm: bone marrow; ha: hydroxyapatite; ha-col: hydroxyapatite-collagen composite; ob: osteoblasts; oc: osteocytes; v: blood vessels. Arrows: lining cells. H&E staining. Bar: 50 μm.

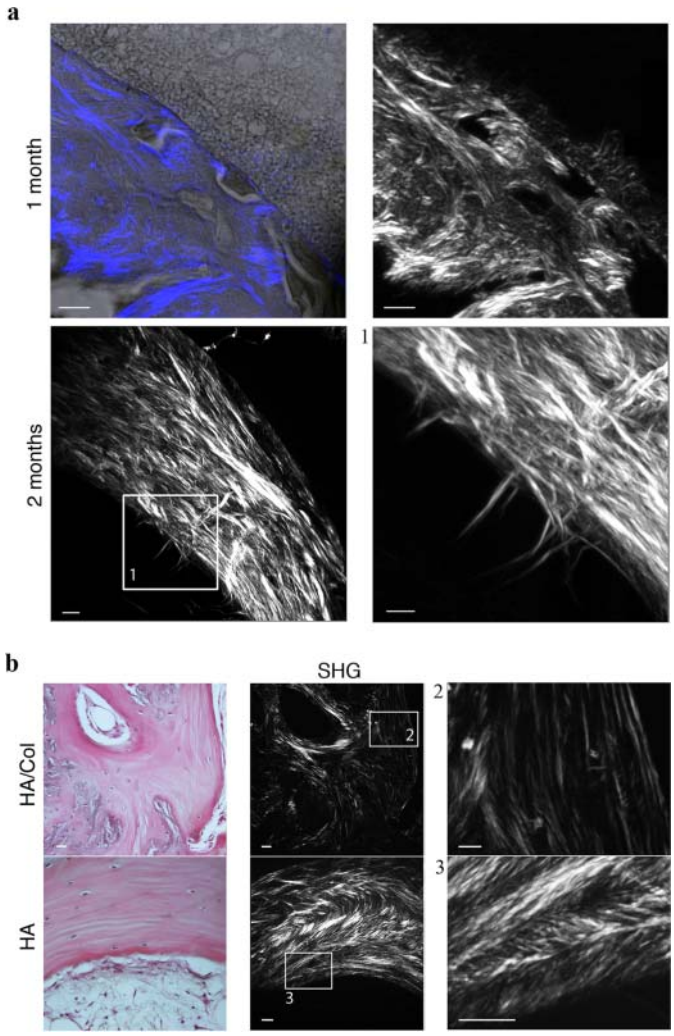

Figure 3 | SHG analysis of bone tissue. (a) collagen fibers within HA scaffold 1–2 months after implantation. The images have been acquired by sequentially scanning the blue channel showing the forward scattered SHG signal and the grey channel showing the transmitted light trough the specimen. The forward scattered SHG signal of different portions of material has been also shown alone. (b) A histological view of the newly formed bone tissue and the corresponding forward scattered SHG signal were shown for both materials 6 months after implantation. Bar: 5 μm.

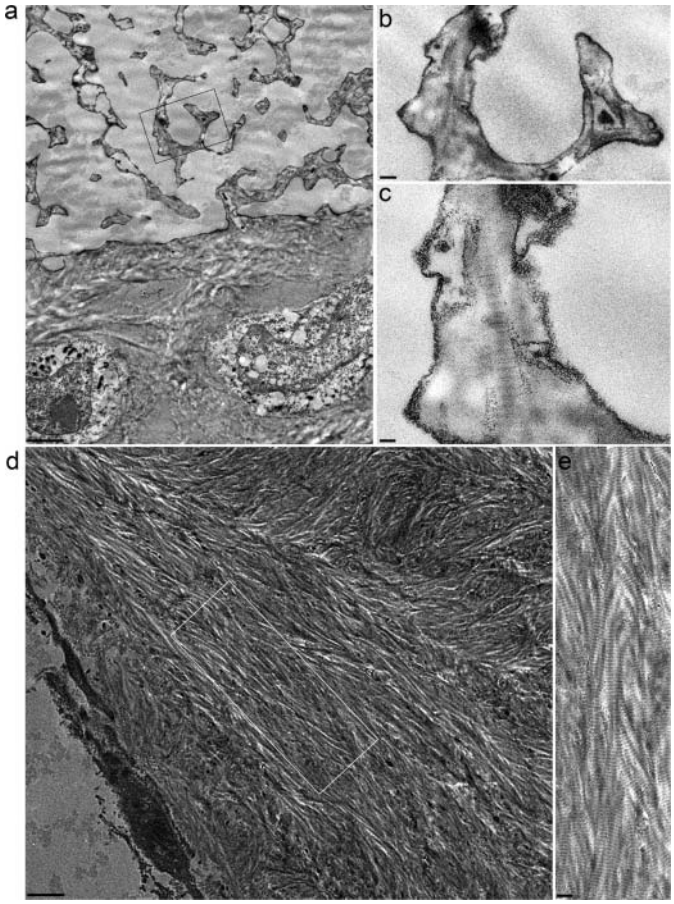

Figure 4 | TEM analysis and collagen pattern within bone tissue. (a) the interface neobone-HA scaffold 2 months after implantation. Note several collagen fibers branching inside the ceramic substitute. (b) and (c) are high magnifications of (a), showing the characteristic banding pattern of the collagen fibrils. (d) shows the organized bone tissue deposited within a representative pore of HA scaffold. Regular series of nested arcs, typical of mature bone tissue, were observed. The inset (e) is an enlarged view of the bone tissue region, where the typical band of collagen fibers is visible. Bars: 2 μm; 0.2 μm; 0.1 μm; 1.25 μm; 0.4 μm.

surface was partially covered by elongated, thin lining cells (arrows). Blood vessels were well represented within the interconnected pores of the ceramic scaffold. At the same experimental time, a significant increase in the amount of neo-formed bone and vascularization could be detected in the HA-Col scaffolds too.

After 6 months, bone formed within the HA scaffolds displayed the typical structure of an ossicle[24], with a marrow cavity filled with hemopoietic cells, adipocytes and formation of functionally active vascular structures, surrounded by concentric lamellae of bone matrix. By contrast, in HA-Col samples, active osteoblasts were still present in the tissue, ready to further deposit new bone matrix. Moreover, large blood vessels were observed randomly pervading the available matrix. In Ha-Col constructs, then, the bone matrix did not display an ordered spatial organization, as shown by an isotropic and un-polarized structure.

Acellular controls of ceramic scaffolds implanted in nude mice did not display any trace of bone tissue during the overall period of observation (data not shown).

The patterns of the bone tissues formed within the different implants were then evaluated at a sub-micrometric scale, with different optical microscopic techniques; related results were combined through a multimodal analysis. The morphology of bone tissue and the collagen fibers organization within HA scaffolds were evaluated through a high-resolution label-free optical microscopic technique (SHG, Second Harmonic Generation)[25,26]. Osteoblasts adherent to the surface of the scaffold primed matrix deposition towards the inner volume of the pore, self-burying inside their lacunae and possibly evolving towards osteocytes (Fig. 3a). Meanwhile, a significant amount of collagen fibers were secreted by the progenitor cells and organized inside the microporosity of the HA scaffold, just beyond the interface scaffold-bone. This result was also confirmed by TEM analysis (see also Fig. 4a–c).

One month later (Fig. 3a), a thicker layer of bone tissue was observed. The collagen fibers displayed a higher level of three-dimensional organization. At the front-end line, where osteoblasts are active in depositing new bone matrix, thick collagen fibers were orthogonal to the direction of bone growth, towards the center of the pore. A compact collagen matrix was also observed, forming a well-organized lamellar structure of concentric layers, parallel to the pore surface.

After six months, we assessed the pattern of bone tissue deposited in both scaffolds (Fig. 3b). In HA-Col bone, the matrix had filled almost all the available volume of the scaffold. In these samples, however, no preferential orientation of collagen fibers was observed

with the exception of small areas, confirming the presence of an isotropic domain characterized by randomly oriented collagen molecules. By contrast, the regular and ordered inner geometry of HA scaffold guided, over time, the bone tissue deposition within the pores. Bone patterns displayed a lamellar structure, with a parallel alignment of collagen fibers organized in concentric layers.

At higher magnification, the forward scattered SHG signal highlighted a high concentration of arched patterns of closely-packed collagen lamellae, corresponding to the regularly varying directions of collagen fibrils within the same bone structure[27]. Cross-striated collagen fibers drawing superposed series of nested arches were observed (Fig. 3b), proving the presence of a cholesteric geometry, as described in compact bone[27].

Ultrathin sections of the fibers observed through the SHG analysis were assessed by TEM microscopy (Fig. 4): fibers infiltrating HA scaffold micropores presented the typical 64 nm banding (Fig. 4a-c), confirming their collagenic nature. TEM also substantiated the presence of regular series of collagenic nested arches (Fig. 4d–e).

Discussion

In the present work, we assessed the pattern of new bone tissue deposited by bone marrow derived cells loaded onto the two scaffolds that maximize differences in internal structure while displaying similar chemical compositions. The chosen murine ectopic model allows bone formation and remodeling virtually in the absence of any mechanical stimulus[28]. In this approach, ceramics offer an osteo-mimetic surface for BMSC to be recognized as a pre-existing bone (osteomimesis) and onto which deposit layer over layer of bone extracellular matrix[12,24]. A preliminary stage of integration between the newly formed bone tissue and the pre-existing ceramic scaffold appeared early after in vivo implantation: such an event was rendered explicit by the consolidation of a thick mesh of collagen fibers infiltrating the micropores of the HA foam. In this respect, we consider that a virtuous circle is established: biomaterials present instructive environments to the cells through chemical and structural cues; the cells, in turn, decode the signals and consequently modulate gene expression and collagen fiber assembly, ultimately modifying the microenvironment and structural nature of the constructs. The osteo-integration progression will then physically consolidate the implanted scaffold and the neo-formed bone in a highly integrated block. This is also in agreement with innumerable instances of cracked spaces found within histological sections of all the HA ceramic retrieved, as previously described[12].

Biomaterial chemistry deeply influences the cell fate at early stages, but the internal architecture of the scaffolds also plays a crucial role, especially at prolonged timings, since it affects bone structure and its deposition kinetics. Indeed, HA and HA-Col based scaffolds generated bone tissues which were different at both morphological-structural scale and molecular level. The events leading to the assembly of collagenous matrices in vivo comprise closely coordinated cellular, enzymatic and self-assembly mechanisms[29]. Procollagens, soluble precursors of fibrillar collagens, are synthesized and secreted into the extracellular matrix and spontaneously assembled into fibrils[30]. TEM analysis of sections of decalcified newly synthesized compact bone revealed collagen fiber patterns characteristic of mature bone. The same results were obtained by the label-free 3D high resolution optical microscopic technique (SHG) applied to thick specimens of engineered bone tissue. HA scaffolds primed progenitor cells to synthesize and deposit collagen fibers as early as few weeks after implantation. At a molecular level, collagen molecules were initially arranged in a nematic phase. The matrix was subsequently remodeled over months, forming higher order and regular structures at the scale of micrometers or more.

As previously described[27], we suggest that the phase transitions could be function of the collagen concentration deposited by the progenitor cells within the scaffolds (Fig. 5). The internal microstructure of HA foam was able to force the co-localization of the collagen fibers synthesized by neighboring cells, triggering bone tissue matrix deposition and assembly processes. Moreover, the HA foam surface controlled the directional apposition of new bony matrix through cell polarization. A spontaneous and complete assembly of collagen molecules, forming regular series of nested arches, was observed. Such pattern is a direct consequence of the organization described in precholesteric-banded patterns and cholesteric phases, and it is also reported as a classical distribution of collagen fibrils in the osteons of compact bone[27,30].

HA-Col scaffolds displayed an apparent linear increase of bone tissue deposition over time; active osteoblasts, in fact, were still visible six months after implantation. The implanted construct and the bone tissue formed a fully integrated bone/scaffold continuum, without any preferential polarization of bone.

Interestingly, in ectopic models, where bone formation mechanisms do not follow the Wolff's law -i.e. when bone formation does not adapt to applied loads[28] - we observed that the tissue remodels itself over time according to the chemical-physical cues given by the scaffold design.

Whenever a regular and geometrically ordered scaffold is presented to the cells as a polarizing template for tissue regeneration, lamellar bone tissue is formed and a continuous twist between collagen fibrils is observed (cholesteric phase), as in compact bone osteons[31,32].

Conversely, in scaffolds with a high level of geometrical complexity, cells do not read a unidirectionally polarizing surface. In fact, in HA-Col scaffolds, even after prolonged time, bone tissue deposition lacks a cholesteric structural organization.

These results confirm that collagen deposition process is somehow influenced by geometry and material composition, which are intimately combined and cross-correlated. Moreover, we consider that the evidences obtained in this study sufficiently support the hypothesis that a different organization of collagen fibers within newly formed bone under unloading conditions can be generated by differently architectured scaffolds. Thus specific chemical-physical conditioning provided by the scaffold design may relevantly contribute to properly drive collagen fibers assembly to target in vivo bone regeneration.

Methods

Scaffold synthesis. Two different scaffolds were used: a highly porous interconnected hydroxyapatite (HA) foam (ENGIpore, Finceramica Faenza, Italy), and a hydroxyapatite-collagen composite sponge (HA-Col/70-30%) (ISTEC-CNR, Faenza, Italy). Both biomaterials were previously chemically and morphologically characterized[21,23]. The composites were examined by scanning electron microscopy (SEM), where SEM is a part of a Dual Beam Instruments 1540XB by Zeiss, with imaging resolution of 1 nm. The images shown here were taken with an acceleration voltage of 10 kV. The sample was at a working distance of about 6 mm and for the best morphological characterization, the detector was Everhardt Thornley that allows for the detection of secondary and backscattered electron.

Osteoprogenitor cell isolation and loading within 3D scaffolds. Ovine bone marrow derived stromal cells (BMSCs) were obtained from the iliac crest of adult female sheeps. Bone marrow aspirate was washed with PBS (phosphate buffered saline) and nucleated cells were isolated using a density gradient solution (Ficoll, Histopaque1; Sigma Chemical, Buchs, CH). Cells were suspended in Dulbecco's modified Eagle's medium (DMEM) supplemented with 10% FCS, 100 IU/mL penicillin, and 100 mg/mL streptomycin and plated at a density of $1*10^6$ cells/cm^2. Medium was changed 2 days after the original plating and then twice a week. When culture dishes were nearly confluent (passage 0), BMSC were detached with 0.05% trypsin-0.01% EDTA and $5*10^5$ cells were replated in 100-mm dishes (passage 1) until the next confluence. Samples of 1.5–2 million of sheep BMSCs were suspended in culture media and statically loaded into porous osteoconductive blocks (cubes of approximately 3 mm side).

In vivo tests. Samples (up to 4 by animal) were subcutaneously implanted in immuno-deficient (ID) (CD-1 nu/nu) mice following an ectopic model of bone formation. Experimental animals were housed and treated in compliance with the actual national and international guidelines (Italian legislative decree 116/92, the European Community Directive 86/609 CEE and FELASA), under the supervision

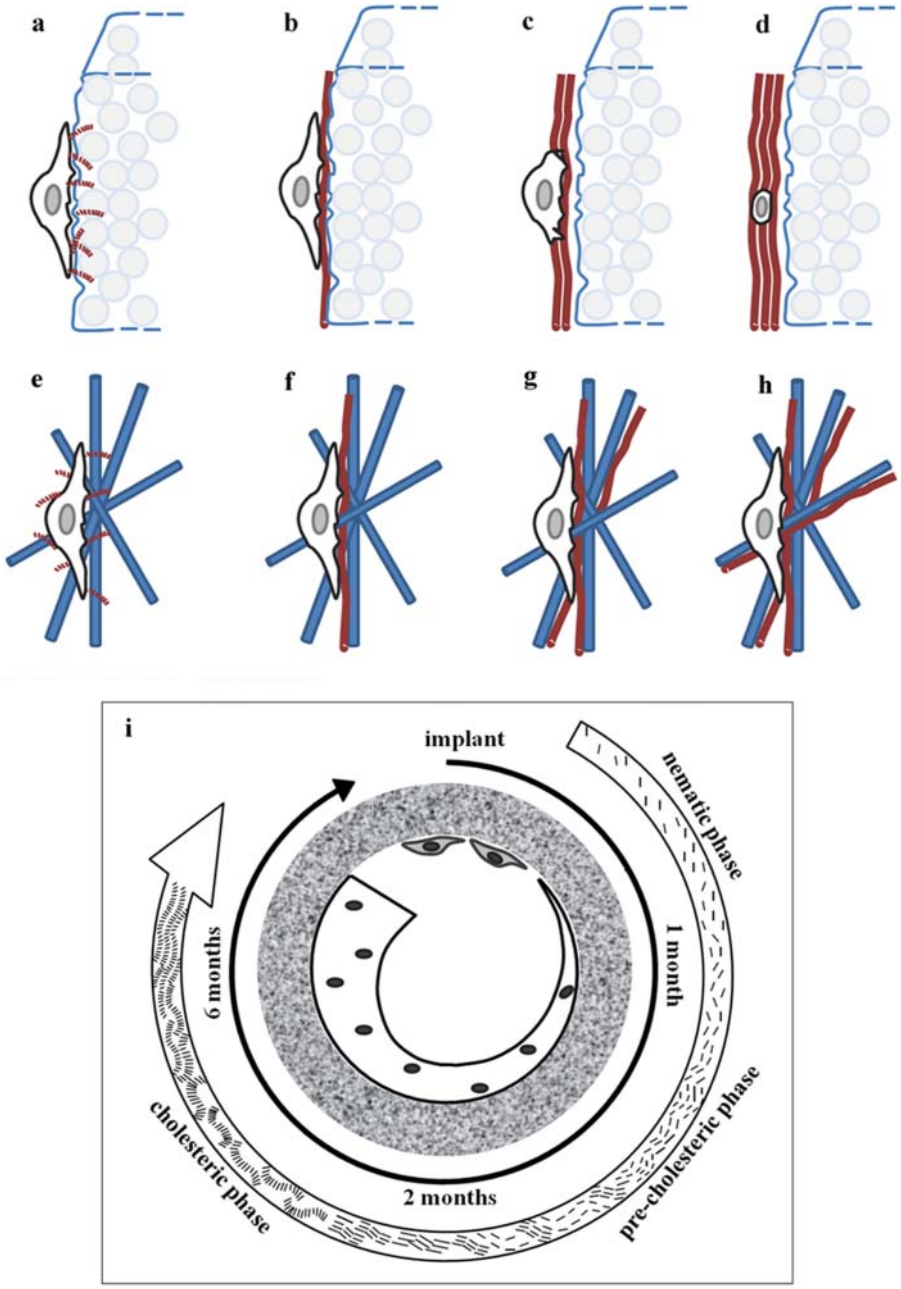

Figure 5 | Model of collagen fibers assembly over time. As soon the osteoprogenitor cell interacts and decodes the ceramic surface (a). it synthesizes and deposits collagen molecules that resemble rods infiltrating the micropores of the HA foam. Cells are therefore induced to deposit newly formed bone tissue in a polarized fashion (b–c–d). On the other side, the nanofibrous Ha-Col sponge offers to the cells a disordered and isotropic microenvironment (e). where deposit collagen fibers in a random 3D geometry (f–g–h). Model showing collagen fibrils assembly in the extracellular matrix by the cells within a HA regular and ordered scaffold is shown (i).

and approval of the Ethical Committee of the National Cancer Research Institute of Genova, Italy, and in accordance to the authorization provided by the Italian Ministry of Health (as of D.M. 146/2009-A and subsequent integrations). Recipient ID 4-wks old female mice, purchased from Charles River Italia (Charles River Lab., Calco, Milan, Italy), were kept in a controlled environment and given free access to food and water. Mice were anesthetized by intramuscular injection of Xilazine (20 mg/ml) and Ketamine (30 mg/ml). Animals were sacrificed 1, 2 or 6 months after implantation. At least three different implants were performed for each time point and for each material type.

Histology and Immunohistochemistry. Grafts were harvested and processed for histological analysis. Briefly, samples were fixed in 4% buffered formalin for 4 h, decalcified with Osteodec (Bio Optica, Milan, Italy) at 37°C for 6 h and dehydrated in ethanol scale for a total of 6 h. Samples were then paraffin embedded, cross-sectioned (5-μm thick) at different levels, stained with both haematoxylin–eosin (H&E) staining. For each scaffold, bone matrix, blood vessels and mesenchymal tissue were evaluated.

SHG microscopy. Second harmonic generation (SHG) imaging microscopy was used to investigate the collagen matrix organization within bone tissue. A SHG and two-photon excitation fluorescence (2PEF) microscope was used for this study. The SHG/2PEF microscope was based on a Leica TCS STED CW, Resonant Scanner Spectral confocal scanning head (Leica Microsystems, Mannheim, Germany). The SHG is collected both in back-scattering (BSHG) and in a transmitted light configuration (forward second harmonic generation; FSHG). Since the excitation wavelength is set at 860 nm, the BSHG spectral component of interest, 415–445 nm, is selected by means of the Leica built-in prism based spectrophotometer, whereas the FSHG is selected by two filters, an IR blocking filter and a 430/30 nm band-pass color filter (HQ430/30 m, Chroma Technology Corp., Bellows Falls, VT, USA)[25]. All panels have been acquired using a 76 nm pixel size and a 100x 1.4 NA oil-immersion objective (HCX PL APO 100x/1.4 Oil, Leica Microsystems, Mannheim, Germany). SHG imaging was used to gather specific organizational motifs, such as the structure of endogenous collagen proteins[26]. Moreover, due to the coherent nature of SHG signal, the intensity of the output is proportional to the square of the local concentration of the proteins observed and is intrinsically 3D.

TEM analysis. Transmission electron microscopy (TEM) was performed retrospectively on formalin-fixed, paraffin-embedded blocks as described[33]. Briefly samples were xylene dewaxed at 60°C, rehydrated through a descending ethanol series, post fixed in 1% OsO4 in distilled water, dehydrated in a graded ethanol series, and embedded in EPON resin. Sections of about 70 nm were cut with a Leica EM UC7 microtome, stained with lead citrate and observed with a JEOL JEM 1011 electron microscope operating at 100 KV.

1. Barrilleaux, B., Phinney, D. G., Prockop, D. J. & O'Connor, K. C. Review: ex vivo engineering of living tissues with adult stem cells. *Tissue Eng* **12**, 3007–3019 (2006).
2. Bianco, P. & Robey, P. G. Stem cells in tissue engineering. *Nature* **414**, 118–121 (2001).
3. Cancedda, R., Bianchi, G., Derubeis, A. & Quarto, R. Cell therapy for bone disease: a review of current status. *Stem Cells* **21**, 610–619 (2003).
4. Livingston, T. L. *et al.* Mesenchymal stem cells combined with biphasic calcium phosphate ceramics promote bone regeneration. *J Mater Sci Mater Med* **14**, 211–218 (2003).
5. Logeart-Avramoglou, D., Anagnostou, F., Bizios, R. & Petite, H. Engineering bone: challenges and obstacles. *J Cell Mol Med* **9**, 72–84 (2005).
6. Oreffo, R. O. & Triffitt, J. T. Future potentials for using osteogenic stem cells and biomaterials in orthopedics. *Bone* **25**, 5S–9S (1999).
7. Cheng, L. *et al.* Osteoinduction of hydroxyapatite/beta-tricalcium phosphate bioceramics in mice with a fractured fibula. *Acta Biomater* **6**, 1569–1574 (2010).
8. El-Ghannam, A. Bone reconstruction: from bioceramics to tissue engineering. *Expert Rev Med Devices* **2**, 87–101 (2005).
9. Kondo, N. *et al.* Osteoinduction with highly purified beta-tricalcium phosphate in dog dorsal muscles and the proliferation of osteoclasts before heterotopic bone formation. *Biomaterials* **27**, 4419–4427 (2006).
10. Ripamonti, U. Osteoinduction in porous hydroxyapatite implanted in heterotopic sites of different animal models. *Biomaterials* **17**, 31–35 (1996).
11. Yuan, H. *et al.* A preliminary study on osteoinduction of two kinds of calcium phosphate ceramics. *Biomaterials* **20**, 1799–1806 (1999).
12. Boyde, A., Corsi, A., Quarto, R., Cancedda, R. & Bianco, P. Osteoconduction in large macroporous hydroxyapatite ceramic implants: evidence for a complementary integration and disintegration mechanism. *Bone* **24**, 579–589 (1999).
13. Kon, E. *et al.* Autologous bone marrow stromal cells loaded onto porous hydroxyapatite ceramic accelerate bone repair in critical-size defects of sheep long bones. *J Biomed Mater Res* **49**, 328–337 (2000).
14. Chang, B. S. *et al.* Osteoconduction at porous hydroxyapatite with various pore configurations. *Biomaterials* **21**, 1291–1298 (2000).
15. Gauthier, O., Bouler, J. M., Aguado, E., Pilet, P. & Daculsi, G. Macroporous biphasic calcium phosphate ceramics: influence of macropore diameter and macroporosity percentage on bone ingrowth. *Biomaterials* **19**, 133–139 (1998).
16. Hollister, S. J., Maddox, R. D. & Taboas, J. M. Optimal design and fabrication of scaffolds to mimic tissue properties and satisfy biological constraints. *Biomaterials* **23**, 4095–4103 (2002).
17. Hutmacher, D. W., Schantz, J. T., Lam, C. X., Tan, K. C. & Lim, T. C. State of the art and future directions of scaffold-based bone engineering from a biomaterials perspective. *J Tissue Eng Regen Med* **1**, 245–260 (2007).
18. Karageorgiou, V. & Kaplan, D. Porosity of 3D biomaterial scaffolds and osteogenesis. *Biomaterials* **26**, 5474–5491 (2005).
19. Li, S., De Wijn, J. R., Li, J., Layrolle, P. & De Groot, K. Macroporous biphasic calcium phosphate scaffold with high permeability/porosity ratio. *Tissue Eng* **9**, 535–548 (2003).
20. Lu, J. X. *et al.* Role of interconnections in porous bioceramics on bone recolonization in vitro and in vivo. *J Mater Sci Mater Med* **10**, 111–120 (1999).
21. Mastrogiacomo, M. *et al.* Role of scaffold internal structure on in vivo bone formation in macroporous calcium phosphate bioceramics. *Biomaterials* **27**, 3230–3237 (2006).
22. Wu, L. & Ding, J. Effects of porosity and pore size on in vitro degradation of three-dimensional porous poly(D,L-lactide-co-glycolide) scaffolds for tissue engineering. *J Biomed Mater Res A* **75**, 767–777 (2005).
23. Tampieri, A. *et al.* Biologically inspired synthesis of bone-like composite: self-assembled collagen fibers/hydroxyapatite nanocrystals. *J Biomed Mater Res A* **67**, 618–625 (2003).
24. Bianco, P. *et al.* Reproduction of human fibrous dysplasia of bone in immunocompromised mice by transplanted mosaics of normal and Gsalpha-mutated skeletal progenitor cells. *J Clin Invest* **101**, 1737–1744 (1998).
25. Bianchini, P. & Diaspro, A. Three-dimensional (3D) backward and forward second harmonic generation (SHG) microscopy of biological tissues. *J Biophotonics* **1**, 443–450 (2008).
26. Campagnola, P. J. *et al.* Three-dimensional high-resolution second-harmonic generation imaging of endogenous structural proteins in biological tissues. *Biophys J* **82**, 493–508 (2002).
27. Giraud-Guille, M. M., Besseau, L. & Martin, R. Liquid crystalline assemblies of collagen in bone and in vitro systems. *J Biomech* **36**, 1571–1579 (2003).
28. Goshima, J., Goldberg, V. M. & Caplan, A. I. The osteogenic potential of culture-expanded rat marrow mesenchymal cells assayed in vivo in calcium phosphate ceramic blocks. *Clin Orthop Relat Res*, 298–311 (1991).
29. Kadler, K. E., Hulmes, D. J., Hojima, Y. & Prockop, D. J. Assembly of type I collagen fibrils de novo by the specific enzymic cleavage of pC collagen. The fibrils formed at about 37 degrees C are similar in diameter, roundness, and apparent flexibility to the collagen fibrils seen in connective tissue. *Ann N Y Acad Sci* **580**, 214–224 (1990).
30. Kadler, K. E., Holmes, D. F., Trotter, J. A. & Chapman, J. A. Collagen fibril formation. *Biochem J* **316 (Pt 1)**, 1–11 (1996).
31. Giraud-Guille, M. M. Twisted plywood architecture of collagen fibrils in human compact bone osteons. *Calcif Tissue Int* **42**, 167–180 (1988).
32. Giraud-Guille, M. M. Twisted liquid crystalline supramolecular arrangements in morphogenesis. *Int Rev Cytol* **166**, 59–101 (1996).
33. Lighezan, R. *et al.* The value of the reprocessing method of paraffin-embedded biopsies for transmission electron microscopy. *Rom J Morphol Embryol* **50**, 613–617 (2009).

Acknowledgements

We thank MIUR for partial funding of the work (Prot. n. RBPR05RSM2; RBIP068JL9). We thank Roberta Martinetti (Finceramica, Faenza, I) for provision of the scaffolds.

Author contributions

S.S., P.G. and R.Q. designed and performed experiments, analysed data and wrote the paper, under the guidance of P.Bianco. S.S., P.G., R.Q. and P.Bianco discussed the results and implications. P.Bianchini conducted SHG characterization of the scaffolds under the guidance of A.D., M.S and A.T. carried out chemical characterization of scaffolds. G.F and U.V. carried out SEM analysis of scaffolds. R.M. conducted TEM analysis. All authors contributed extensively to the work presented in this paper.

Additional information

Competing financial interests: The authors declare no competing financial interests.

How to cite this article: Scaglione, S. *et al.* Order versus Disorder: in vivo bone formation within osteoconductive scaffolds. *Sci. Rep.* **2**, 274; DOI:10.1038/srep00274 (2012).